International Journal of Heat and Mass Transfer 52 (2009) 5451–5458

Contents lists available at ScienceDirect

International Journal of Heat and Mass Transfer

journal homepage: www.elsevier.com/locate/ijhmt

Design method of automatic energy transport devices based on the thermomagnetic effect of magnetic fluids

Wenlei Lian, Yimin Xuan *, Qiang Li

School of Power Engineering, Nanjing University of Science & Technology, Nanjing 210094, China

ARTICLE INFO

Article history:
Received 8 February 2009
Received in revised form 14 May 2009
Accepted 17 June 2009
Available online 7 August 2009

Keywords:
Magnetic fluid
Thermomagnetic effect
Automatic energy transport

ABSTRACT

The present work is aimed at developing a design method for automatic energy transport devices based on the thermomagnetic effect of magnetic fluids. A model for describing thermomagnetic convection of a temperature-sensitive magnetic fluid in a loop is established, which includes the coupling of the three fundamental phenomena, i.e. magnetic, thermal, and fluid dynamic features. The thermomagnetic convection of the temperature-sensitive magnetic fluid in a loop-shape energy transport device is simulated in the presence of an external magnetic field. Comparison between experimental data and numerical results is carried out to validate the model. The effects of different factors such as input heat load, heat sink temperature and magnetic field distribution along the loop on the performance of the energy transport device are analyzed and discussed according to the numerical simulation results.

1. Introduction

Magnetic fluid is a colloidal suspension consisting of carrier liquid and magnetic nanoparticles. It possesses not only the flowability of common Newtonian fluids, but also the magnetic features being similar to those of the bulk magnetic materials [1–4], which reminds us of applying magnetic fluids to controllable thermal processes. Among this type of functional fluids, the temperature-sensitive magnetic fluid induces greater research impulse because of its temperature-dependent magnetization feature and thermomagnetic effect [5–7]. When the temperature-sensitive magnetic fluid experiences a temperature variation in the presence of an external magnetic field, the balance of the fluid magnetization will be broken and a thermomagnetic driving force is produced. The consequence is straightforward: the fluid can be driven under such field induced thermomagnetic force, which implies that it is possible that heat is directly converted to kinetic energy. It may be promising and fascinating to apply such an energy conversion principle in a variety of fields, for example, thermal management system for some specialized purposes without installing any pumps or converting waste heat into useful power, which is extremely important for the sustainable development of energy. One may find some publications on investigation efforts on different energy conversion devices based on the thermomagnetic effect of temperature-sensitive magnetic fluids [8–10]. This type of energy conversion devices using magnetic fluid is even more attractive for space use or in a situation where no maintenance may be required.

With urgent need for developing this type of energy conversion devices, however, the suitable method for designing such devices is still lacking and the relevant references regarding the mechanism of thermal convection in energy conversion devices with magnetic fluids are relatively sparse. The insightful knowledge on the relationship among an imposed magnetic field, the magnetic fluid flow, and the temperature distribution of the magnetic fluid is still lacking. This paper is focused upon the constitutive features of thermal, flow and magnetic field associated with the thermomagnetic convection of magnetic fluids in order to get insight into the operation mechanism of energy conversion devices based on magnetic fluids. Firstly, the model of the thermomagnetic convection of magnetic fluids is established to couple the three fundamental features of magnetic, thermal, and fluid dynamic phenomena. Based on the model, we numerically simulate the thermomagnetic convection behaviors of a kerosene-based temperature-sensitive magnetic fluid in the presence of an external magnetic field inside an energy transport or conversion device loop. Secondly, some detailed discussions on the operation mechanism of such a device are conducted from the numerical simulation results. Finally, we validate this model by comparing the numerical results with the experimental observations.

2. Mathematical model and numerical simulation

2.1. Mathematical model

A Cartesian coordinate system is used for the mathematical model. The direction of gravity is along the negative y direction.

* Corresponding author.
E-mail address: ymxuan@mail.njust.edu.cn (Y. Xuan).

0017-9310/$ - see front matter © 2009 Elsevier Ltd. All rights reserved.
doi:10.1016/j.ijheatmasstransfer.2009.06.031

Nomenclature

A	area (m^2)	W	work (J)
$\boldsymbol{B}$	magnetic induction ($N\,A^{-1}\,m^{-1}$)	λ	thermal conductivity ($W\,m^{-1}\,K^{-1}$)
C	specific heat capacity ($J\,kg^{-1}\,K^{-1}$)	λ_c	thermal conductivity of the base liquid ($W\,m^{-1}\,K^{-1}$)
$\boldsymbol{f}$	force density ($N\,m^{-3}$)	λ_p	thermal conductivity of the magnetic nanoparticle ($W\,m^{-1}\,K^{-1}$)
$\boldsymbol{f_\eta}$	viscosity force density ($N\,m^{-3}$)	μ	dynamic viscosity ($N\,s\,m^{-2}$)
$\boldsymbol{f_m}$	magnetization force density ($N\,m^{-3}$)	μ_0	permeability of free space ($N\,A^{-2}$)
$\boldsymbol{g}$	acceleration of gravity ($m\,s^{-2}$)	φ	magnetic scalar potential (A)
$\boldsymbol{H}$	magnetic field intensity ($A\,m^{-1}$)	ϕ	solid volume fraction
H	scalar magnitude of magnetic field intensity ($A\,m^{-1}$)	ϕ_m	solid mass fraction
K	pyromagnetic coefficient ($A\,m^{-1}\,K^{-1}$)	η	dynamic viscosity ($N\,s\,m^{-2}$)
M	scalar magnitude of magnetization ($A\,m^{-1}$)	η_c	viscosity of the base liquid ($N\,s\,m^{-2}$)
p	pressure (Pa)	η_0	viscosity of the colloid ($N\,s\,m^{-2}$)
P	electric power (W)	η_H	viscosity of the colloid in the presence of a magnetic field ($N\,s\,m^{-2}$)
T	temperature (K)	ρ	mass density ($kg\,m^{-3}$)
$\boldsymbol{V}$	velocity vector ($m\,s^{-1}$)		
V_x	velocity component ($m\,s^{-1}$)		

To establish a model for the thermomagnetic convection of temperature-sensitive magnetic fluids, the fluid is assumed as a single-phase Newtonian fluid. According to Neuringer and Rosensweig's work [11], this assumption is proper for description of dynamic phenomena of the magnetic fluid from the macroscopic view. For simulating the thermomagnetic convection of the single-phase magnetic fluid along a loop (as shown in Fig. 1), the following governing differential equations in the presence of an external magnetic field yield as:

Equation of continuity:

$$\nabla \cdot \boldsymbol{V} = 0 \tag{1}$$

Equation of motion:

$$\rho(\boldsymbol{V}\cdot\nabla)\boldsymbol{V} = \rho\boldsymbol{g} + \boldsymbol{f}_m - \nabla p + \boldsymbol{f}_\eta \tag{2}$$

Equation of energy conservation [12]:

$$\rho C(\boldsymbol{V}\cdot\nabla)T + \mu_0 T\frac{\partial M}{\partial T}(\boldsymbol{V}\cdot\nabla)H = \nabla\cdot(\lambda\nabla T) \tag{3}$$

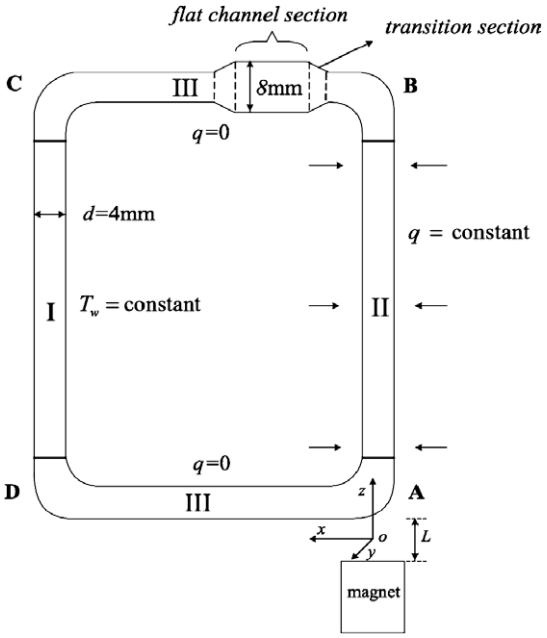

Fig. 1. Schemetic fluid loop used in simulation.

where the quantity M represents the scalar magnitude of the magnetization, H indicates the scalar magnitude of field intensity, C is the specific heat, and λ is the thermal conductivity. The vectors $\rho\boldsymbol{g}$, $\boldsymbol{f}_\eta$ and $\boldsymbol{f}_m$ in Eq. (2) are the gravity force, the viscosity force, and the magnetization force, respectively. It is clear that the second term in Eq. (3) is the energy associated with the magnetic field, which may be equal to zero for a time-independent magnetic field.

For a unit volume of the magnetic fluid, the work differential is given [13]

$$\delta W = -\mu_0 H\left[\left(\frac{\partial M}{\partial H}\right)_T dH + \left(\frac{\partial M}{\partial T}\right)_H dT\right] \tag{4}$$

and the magnetic force experienced can be derived as:

$$\boldsymbol{f}_m = \mu_0 M\nabla H + \mu_0 H\frac{\partial M}{\partial T}\nabla T \tag{5}$$

It is well known that the temperature variation in the temperature-sensitive magnetic fluid will lead to a change in the magnetization and affect the magnetic force acting on the fluid system in the presence of an external magnetic field. As a whole, the governing equations are strongly coupled. The fluid flow affects convective heat transfer and temperature distribution inside the magnetic fluid and thereby affects the driving force on the fluid. On the other hand, the fluid temperature distribution can induce the magnetization variation of the magnetic fluid and then may alter the driving force. To figure out the driving force acting on the fluid subjected to an inhomogeneous magnetic field, the intensity distribution of the external magnetic field should first be determined.

2.2. Computation of the magnetic field distribution

As a magnet is positioned on or nearby the loop, the magnetic field along the loop is fixed. Here a method for computing the intensity distribution of a static magnetic field is introduced by taking a practical cylindrical Nd–Fe–B magnet as an example. The magnet is placed nearby the flow loop (as shown in Figs. 1 and 2). The Maxwell equations for a static magnetic field in the free space are written as follows:

$$\nabla\cdot\boldsymbol{B} = 0 \tag{6}$$

$$\nabla\times\boldsymbol{H} = 0 \tag{7}$$

The magnetic induction $\boldsymbol{B}$ and the magnetic field vector $\boldsymbol{H}$ are related by the constitutive relation:

$$\boldsymbol{B} = \mu_0\boldsymbol{H} \tag{8}$$

where μ_0 is a magnetic permeability in vacuum.

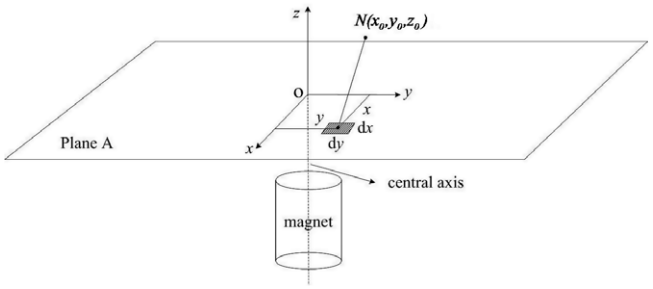

Fig. 2. Green function method for the solution of Laplace's equation.

The magnetic scalar potential φ is defined as

$$\boldsymbol{H} = -\nabla\varphi \tag{9}$$

and the potential function φ obeys to the Laplace's equation

$$\nabla^2\varphi = 0 \tag{10}$$

It is convenient to apply Green function method to solving the boundary-value problem of Laplace's Eq. (10) in a half-space. Therefore, what is needed is to find the solution to the following equation (here the Cartesian coordinates is introduced):

$$\frac{\partial^2\varphi}{\partial x^2} + \frac{\partial^2\varphi}{\partial y^2} + \frac{\partial^2\varphi}{\partial z^2} = 0, \quad z > 0 \tag{11}$$

with the following boundary condition:

$$\varphi|_{z=0} = f(x,y) \tag{12}$$

As a cylinder magnet is involved, we consider a perpendicular plane (hereafter referred to as plane A) to the axis of the cylinder as the boundary of the half-space, which is 2 mm away from the magnet (as shown in Fig. 2). The length of the magnet is 70 mm and the diameter of the cross-section is 30 mm. Consider z axis along the central axis of the cylindrical magnet and the origin of the coordinate system is coincident with the intersection between the axis and plane A. By means of the Green function method, the value of φ at a given point $N(x_0, y_0, z_0)$in the half-space above the plane ($z > 0$) can be figured out with the following integral:

$$\varphi(x_0,y_0,z_0) = \frac{1}{2\pi}\int_{-\infty}^{\infty}\int_{-\infty}^{\infty}\frac{z_0}{\left[(x-x_0)^2+(y-y_0)^2+z_0^2\right]^{\frac{3}{2}}}f(x,y)\,dx\,dy \tag{13}$$

once the scalar distribution of magnetic potential on the boundary plane $f(x, y)$ is known.

The magnetic induction $\boldsymbol{B}$ within an area with the dimensions of $-200 < x < 200$ (mm) and $-200 < y < 200$ (mm) in plane A can be measured with 1 mm increment along each direction (x and y) by using a Teslameter. The Teslameter is provided by LAKESHORE Inc. and the accuracy of it is ±2%. The readings range from a large value to zero (at the boundary of the measured area). The values of field intensity $\boldsymbol{H}$ at these discrete points are easily obtained from Eq. (8). By defining the scalar magnetic potential φ at the point ($x = 200$, $y = 200$) as zero, the values of φ at the measuring points are determined from Eq. (9). Fig. 3 illustrates the distribution of φ along the x axis ($y = 0$). Therefore, the curve for φ along the x axis ($y = 0$) can be fitted as the following function with an acceptable discrepancy:

$$\varphi = 0.047 + 5448.4 \times \exp\left(-\frac{x^2}{482.98}\right) \tag{14}$$

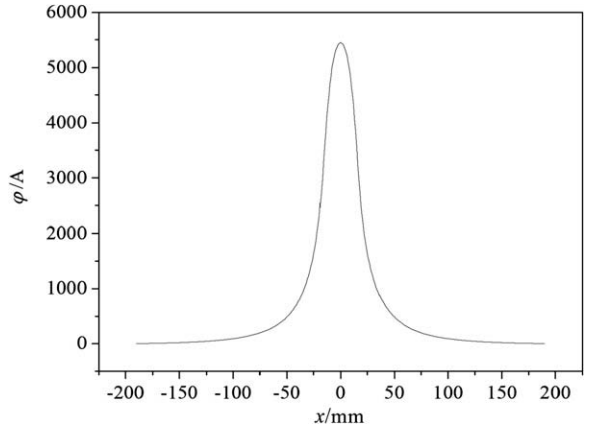

Fig. 3. Distribution of potential φ along the x axis ($y = 0$).

Due to the axial symmetry of the magnetic field, the distribution of φ within plane A can be expressed as:

$$f(x,y) = 0.047 + 5448.4 \times \exp\left[-\frac{(x+y)^2}{482.98}\right] \tag{15}$$

By substituting Eq. (15) into Eq. (13), the scalar magnetic potential at point N can be numerically calculated. Furthermore, the field intensity component can be figured out from the φ values corresponding to the adjacent points. As a result, the magnetic field distribution in this half-space is determined (it should be clear that the magnetic fluid is often placed within such a half-space, i.e. one side of the magnet). The advantage of introducing the analytical calculation of the magnetic field is that one can easily get the magnetic field intensity and the relevant properties such as the field gradient in any computational regions or grids if only the coordinates are given.

It should be clear that the magnetic field obtained by using the above-mentioned method, which is produced by the permanent magnet, is an applied external field, $\boldsymbol{H_e}$, in the air in which the magnetic fluid is placed. However, Eqs. (1)–(5) take the magnetic field, $\boldsymbol{H}$, to be the field inside the magnetic fluid. The magnetic field inside the magnetic material differs from the applied field by inclusion of the demagnetization field:

$$\boldsymbol{H_i} = \boldsymbol{H_e} - D\boldsymbol{M} \tag{16}$$

where $\boldsymbol{H_i}$ is the field inside the fluid, $\boldsymbol{H_e}$ is the externally applied field and $\boldsymbol{M}$ is the magnetization. In the present work, $\boldsymbol{H_e}$ is produced by the permanent magnet and the calculation of it has been explained in this section. $\boldsymbol{M}$ is determined from an empirical formula by using $\boldsymbol{H_e}$, which will be performed in the next section. So that the magnetizing factor D is needed for calculation of the magnetic field inside the fluid.

It is very difficult to determine the magnetizing factor of the magnetic material if the shape of it is not an oblate ellipsoid or a cylinder [14–16]. Here an approximation of the magnetizing factor is estimated by considering the special shape of the fluid. Since the fluid forms a closed loop in the channel, we consider the magnetizing factor along the axial direction of the tube as zero, and the factors along each of the other two directions as 0.5 due to the symmetry of the circular cross-section of the tube (the change of the cross-section at the flat section is neglected for simplification). And then the field inside the fluid is obtained by using Eq. (16).

2.3. Properties of the magnetic fluid

Since the magnetic fluid is assumed to be a single-phase mixed medium in this model, some parameters of the fluid should be

determined according to the properties of the magnetic nanoparticles and the liquid base as well as their compositions. In this study, a kerosene-based Mn–Zn ferrite magnetic fluid is used with saturation magnetization 6.5×10^4 A m^{-1}. The averaged diameter of the suspended magnetic particles is about 6.8 nm and the volume fraction of ferrite magnetic nanoparticles is 0.045.

Thermal conductivity of the magnetic fluid is approximately calculated by the known Maxwell formula:

$$\lambda = \lambda_c \left[1 - \frac{3(\lambda_c - \lambda_p)\phi}{2\lambda_c + \lambda_p + \phi(\lambda_c - \lambda_p)}\right] \tag{17}$$

Where λ_c is the thermal conductivity of the base liquid and λ_p is the particle thermal conductivity. Here the quantity ϕ represents the volume fraction of magnetic nanoparticles suspended inside the magnetic fluid.

Another important thermal parameter of the magnetic fluid is heat capacity and it is determined from the following expression:

$$C = C_p\phi_m + C_c(1 - \phi_m) \tag{18}$$

where C_p and C_c are the specific heat values of magnetic nanoparticles and base liquid, respectively, and ϕ_m represents the mass concentration of the magnetic nanoparticles.

Calculation of the viscosity $\eta(H, T)$ of temperature-sensitive magnetic fluid in the presence of an external magnetic field is somewhat complicated. The viscosity η_0 of magnetic fluid with no external magnetic field can be described with the well-known Einstein formula:

$$\eta_0 = \eta_c\left(1 + \frac{5}{2}\phi\right) \tag{19}$$

where η_c is the dynamic viscosity of the base liquid.

The temperature-dependent viscosity of the base liquid takes the form as [17]

$$\eta_c = y_0 + a\exp\left(\frac{b}{T}\right) \tag{20}$$

For the sample fluid, these coefficients are determined from the experimental data as $y_0 = 0.005$ N s m^{-2}, $a = 1.54 \times 10^{-7}$ N s m^{-2} and $b = 2.54 \times 10^3$ K. Obviously, the feature of the temperature-dependent viscosity of base liquid governs the temperature dependence of the viscosity of the magnetic fluid.

Substitution of (20) in (19) leads to the expression

$$\eta_0 = \left(1 + \frac{5}{2}\phi\right)\left[y_0 + a\exp\left(\frac{b}{T}\right)\right] \tag{21}$$

One may find various correlations about the magnetic field-dependent viscosity $\eta(H, T)$ of magnetic fluids such as linear proportion, exponential, or even more complicated relations in the literature [18–20]. In this work, we use the following linear correlation obtained from our experimental data:

$$\eta(H_e, T) = \eta_0 + \eta_0 cH_e = (1 + cH_e)\eta_0 \tag{22}$$

where η_0 denotes the magnetic fluid viscosity in the absence of an external magnetic field, H_e is the magnitude of the externally applied field, c is a constant with its value equal to 0.007 and the field intensity H_e in the above equation is in the range of 0–500 Oe since the viscosity reaches a saturation point above this range.

By substituting (21) into (22), the magnetic fluid viscosity of taking the magnetic field effect and thermomagnetic effect into account can be expressed as follows:

$$\eta_H = \eta(H_e, T) = (1 + cH_e)\left(1 + \frac{5}{2}\phi\right)\left[y_0 + a\exp\left(\frac{b}{T}\right)\right] \tag{23}$$

Among the properties of the magnetic fluid, the most important one is the fluid magnetization which is a function of the magnetic field intensity and fluid temperature. Vislovich [21] proposed the following relationship between the fluid magnetization and the external magnetic field:

$$M = M_s\frac{H_e}{H_T + H_e} \tag{24}$$

where M_s is the saturation magnetization of the magnetic fluid and H_T is the magnetic field intensity at which the fluid magnetization is equal to $M_s/2$.

In fact, Eq. (24) is obtained by fitting with the M–H curve for actual magnetic fluids. By taking the effect of the fluid temperature variation on the magnetization into account, the expression for the fluid magnetization M becomes:

$$M = M_s\frac{H_e}{H_T + H_e} - K(T - T_0) \tag{25}$$

where the pyromagnetic coefficient K is defined as $K = -(\frac{\partial M}{\partial T})_H$ and T_0 is the reference temperature (here it is set to be the room temperature 298 K). The pyromagnetic coefficient indicates the temperature dependence of the magnetic fluid magnetization and can be determined from the slope of the M–T curve obtained with the experimental data. Usually, this parameter can be assumed to be constant within the operating temperature range. Table 1 lists the properties of the sample fluid. The M–H and M–T curves of the studied fluid were determined by using a Vibrating Sample Magnetometer (LAKESHORE Inc, LS307-9309) with an accuracy of 2%. The maximum applied magnetic field of the VSM is up to 20 KOe, the resolution is ±0. 005% and the sensitivity is 5 μemu.

2.4. Numerical computation

By means of the above-mentioned model, numerical computation is carried out to simulate the performance of a loop-shape energy transport device. Fig. 1 schematically depicts the geometry of the fluid loop and positions of heat source, heat sink, and magnet involved in simulation. The geometry is an 85 mm × 70 mm loop and the cross-section of the fluid is a 4-mm diameter tube except at the flat channel section which has a rectangular cross-section. The flat channel section has dimensions of 8 mm in width (direction z), 16 mm in length (direction x) and 0.5 mm in depth (direction y). In addition, there are two gradual transition sections between the flat channel and the cylindrical channel and each of them is 4 mm in length. The Nd–Fe–B magnet is located at a position being L mm (the distance L is adjustable) away from the loop and its central axis is along the channel axis to provide inhomogeneous magnetic field.

The whole loop is divided into three different types of segments which are labeled as I, II, and III, respectively. No-slip boundary conditions are applied to the channel walls. As for the thermal boundary conditions, the boundary condition of constant surface temperature is applied to the channel wall in segment I where the heat sink with low temperature is installed, the boundary condition of a uniform surface heat flux is imposed on the channel wall in segment II where the heat source with input heat flux is emplaced, and the channel wall in segment III is thermally insulated.

Table 1
Properties of the sample fluid (kerosene-based Mn–Zn ferrite magnetic fluid).

Property	Value	Property	Value
λ_c (W m^{-1} K^{-1})	0.113	C_c (J kg^{-1} K^{-1})	2090
λ_p (W m^{-1} K^{-1})	6	C_p (J kg^{-1} K^{-1})	620
λ (W m^{-1} K^{-1})	0.18	C (J kg^{-1} K^{-1})	1826
K (A m^{-1} K^{-1})	1050		

The numerical calculation is carried out by using the SIMPLE method for the system of equations. As for the discretization of the domain, second-order upwind was used for the flow and energy equations. To divide the geometry into discrete control volumes, about 1.5×10^5 tetrahedral computational cells, 2.8×10^5 triangular elements, and more than 3.5×10^4 nodes were used for the loop. Initially, the magnetic fluid inside the whole loop is stationary and the loop system is at the thermal equilibrium state with temperature 298 K. As the initialization was carried out, the external magnetic field values were calculated at each computational cell, which would be used in the later iteration process for calculating the source terms.

3. Results and discussions

Once the external magnetic field is exerted on the loop system and the heat source and sink are put into operation, the magnetic fluid commences to flow within the channel under the magnetic field and the temperature gradient inside the fluid. Computation has revealed that if all operating conditions are fixed, a stable circulation flow of the magnetic fluid can be maintained inside the loop at a fixed heat load after the whole system starts. Adjusting the operating conditions of the device will alter the flow and temperature distribution of the magnetic fluid in the loop.

3.1. Thermomagnetic convection subjected to different heat flux

By maintaining the wall temperature T_{hs} of cooling section (segment I) at 273 K, we have numerically investigated the performance of the automatic energy transport device for different heat loads. The distance between the magnet and the loop L is 5 mm here.

The velocity vectors of the magnetic fluid in the cross-section of the flat channel are illustrated in Fig. 4. Obviously, the axial velocity component is dominant in the central section of the flat channel, which means that the fully-developed flow appears in this section. Since different heat loads from the heat source section will lead to variation of the temperature and magnetization of the magnetic fluid along the loop, the consequent variation of the driving force will influence the fluid flow. Fig. 5 shows the peak value of velocity V of the magnetic fluid as a function of the input heat flux, which indicates that flow velocity of the magnetic fluid increases with the input heat flux.Fig. 6 illustrates the contour of the fluid temperature at the heat load $q = 3000\ \mathrm{W/m^2}$. Evidently, hotter magnetic fluid from the heat source section flows through channel DA, transports heat from the heater to the heat sink, and flows back the heat source section, so that the flow circulation of the magnetic fluid inside the loop is maintained. Fig. 7 illustrates variations of the fluid temperature T_L at the outlet of the cooling section and T_H at the outlet of the heating section as well as the temperature differences ΔT between them, respectively. For a fixed temperature of the heat sink section, the temperature difference ΔT increases with increases in the exerted heat load. As the temperature difference ΔT increases, the magnetization of the magnetic fluid experiences increasing variation, and then the flow velocity of the fluid increases.

These findings show us that for the automatic energy transport device depicted in Fig. 1 the uneven temperature distribution or temperature gradient resulting from heat loads can induce flow of the magnetic fluid in the loop and the flow velocity increases with increase in the input heat load. It is implied that such a device may be used as an automatically-cooling device whose performance is of self-control function corresponding to the input heat load. As the heat load on the loop rises, the magnetic fluid circulates at a higher velocity in the loop and heat will be more quickly transported from the heating section to the cooling section, and vice versa.

3.2. Effect of cooling condition on the device performance

Besides the heat load, the heat sink temperature also affects the flow velocity of the magnetic fluid in the loop because of the fact that the cooling condition of the heat sink influences the fluid temperature distribution which is associated with the magnetic driving force. By keeping the heat flux from the heating section $q = 3000\ \mathrm{W/m^2}$, Fig. 8 illustrates the fluid velocity V subjected to different heat sink temperature T_{hs}. The distance between the magnet and the loop L is 5 mm here. It is shown that as the heat sink temperature increases, the thermomagnetic flow slows down. The reason consists in that for a given heat load at the heat source section, increase in the heat sink temperature degrades the cooling performance of the device, so that the fluid temperature at the heat source section as well as at other sections of the whole loop remarkably increases, which debases the fluid magnetization and magnetic driving force. Although the temperature difference ΔT shows an increase with increase in the heat sink temperature (as shown in Fig. 9), such change is limited within a small range that it may have little influence on the magnetic driving force. On the other hand, decline of the flow velocity may attribute to further decrease in the fluid magnetization as the heat sink temperature increases. Compared with the heat load, the influence of heat sink temperature on the flow velocity is smaller. However, it is still important to select a heat sink of the suited temperature for the device performance because a higher heat sink temperature will leads to a higher fluid temperature within the whole loop, which is less beneficial for cooling performance of the device.

3.3. Effect of magnetic field on the device performance

Since an earth magnet is used to provide external magnetic field, both the field intensity and field gradient imposed on the fluid will decrease if the distance between the magnet and the loop L increases. While keeping the heat load $q = 3000\ \mathrm{W/m^2}$ and the heat sink temperature $T_{hs} = 273$ K, we have numerically investigated the effect of the distance L on the flow velocity of the magnetic fluid in the loop.

It is found that the flow velocity of the magnetic fluid in the loop shows a strong dependence on the external magnetic field. As shown in Fig. 10, an increase in the distance L considerably reduces the flow velocity. It can be concluded that the driving force acting on the magnetic fluid decreases as L increases, even if ΔT show an obvious increasing tendency during operation (as shown in Fig. 11). This reveals the fact that a wider distance between the magnet and the loop leads to decrease in strength of the magnetic field imposed on the fluid. As the magnet moves far away from the loop, this trend will continue until the magnetic force no longer has the ability to drive the fluid.

It is clear that a stronger magnetic field exerted on the fluid loop and/or a better matching between the magnetic field distribution and the temperature field of the fluid will conduce to a robust device with better performance. Therefore, attention should be paid to the integrative design of the magnetic field, heat source, and heat sink to realize the synergy between the magnetic field and the temperature distribution of the fluid in the loop for actualizing an as large driving force as possible.

4. Model validation

Some experimental investigations on such kind of loop have been carried out in our previous work [22–24]. We use the same

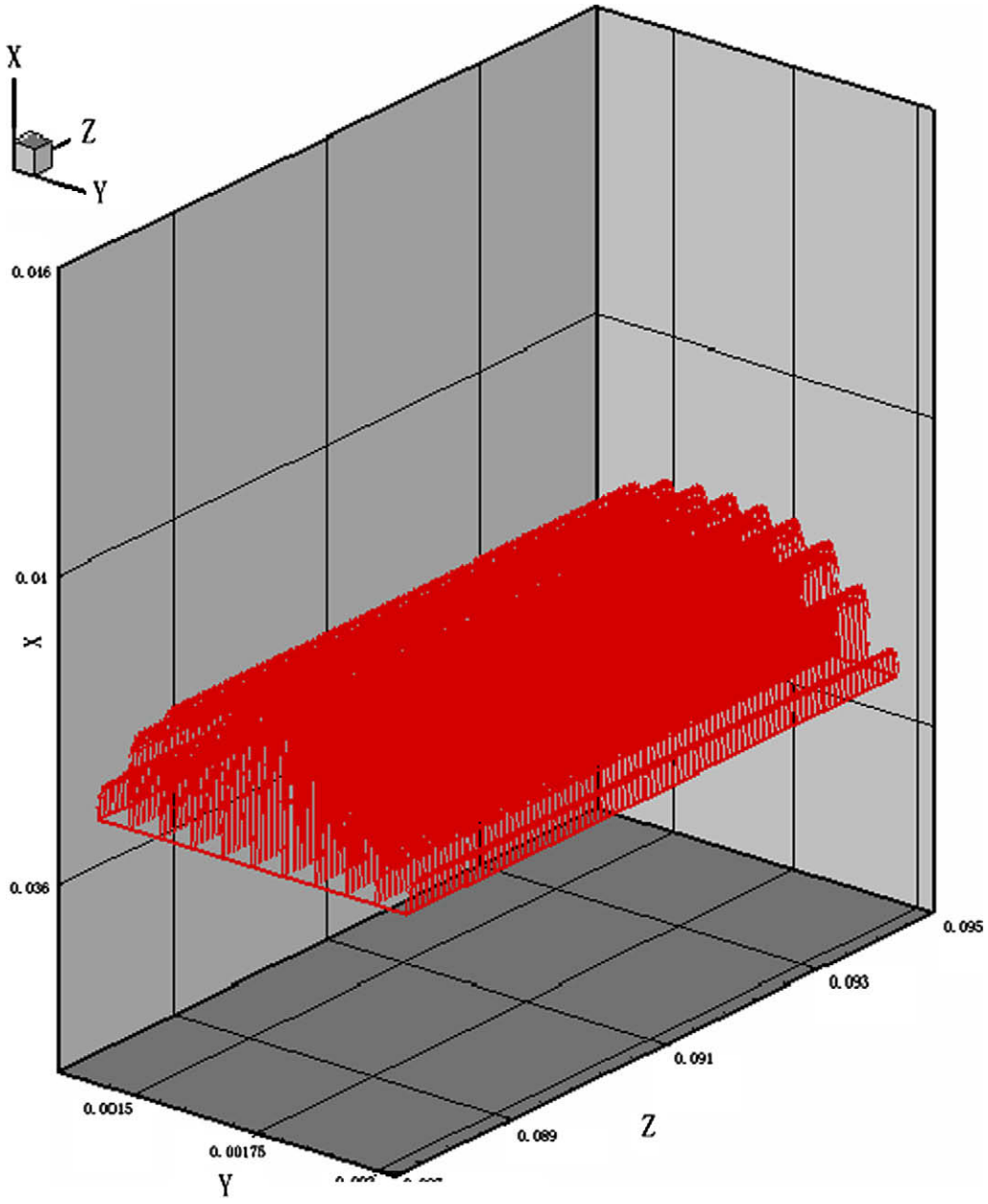

Fig. 4. Velocity vectors of the fluid in the flat channel section.

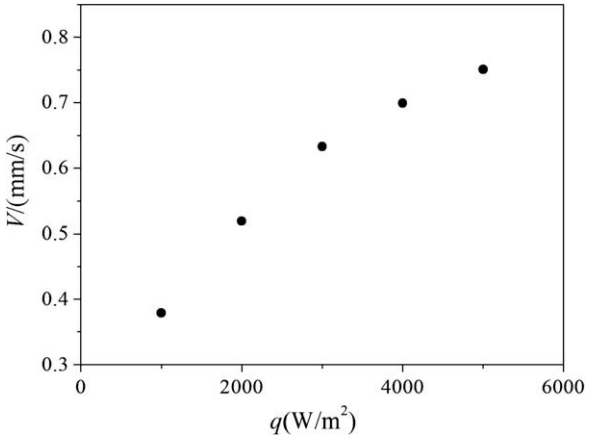

Fig. 5. Velocity of the magnetic fluid subjected to different heat flux.

experimental methods including the flow velocity measurement and temperature measurement in the present work for validating the proposed model and the numerical simulations. The channel loop is mainly made of a 4-mm diameter glass tube. A direct current (DC) heater is used as the heat source which is wrapped around the glass tube. A cooling chamber is integrated with the loop through which the coolant of ethylene glycol (being cooled by a constant low-temperature bath with a fine control uncertainty of ±0.1 K) circulates as the heat sink. The calibrated K-type thermocouples are used to measure the fluid temperature measurements at the heating section and cooling section. The system is thermally insulated with sponge to reduce the heat loss from the loop to the ambient except of the flat channel section for flow visualization, which is an aluminum-based channel with an optical glass cover attached to the channel top surface by glue. The particle image velocimetry (PIV) system is used to record the flow field at the flat channel section.

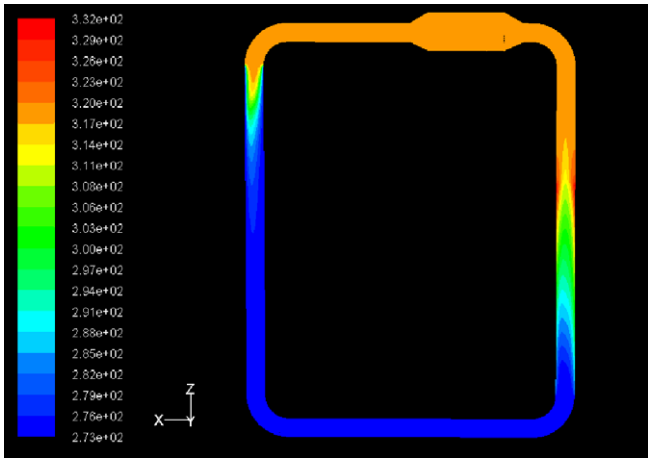

Fig. 6. Contour of the fluid temperature.

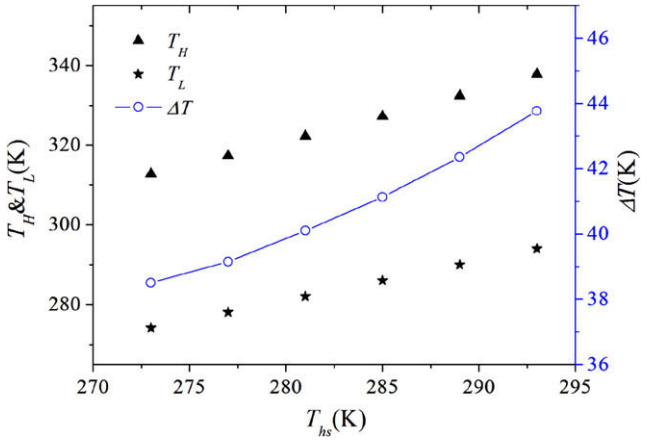

Fig. 9. Temperature variation with heat sink temperature.

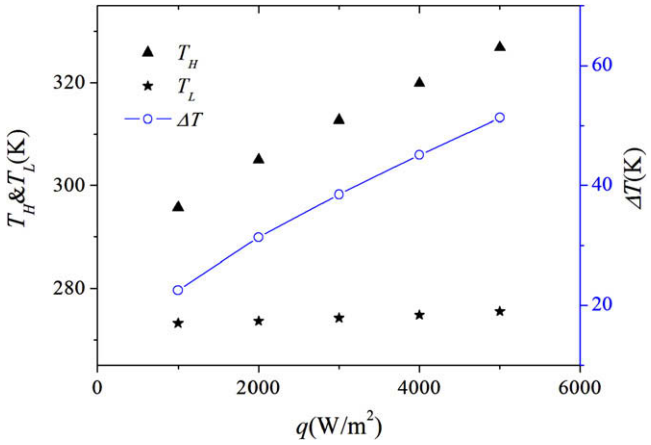

Fig. 7. Fluid temperature variation with heat load on the loop.

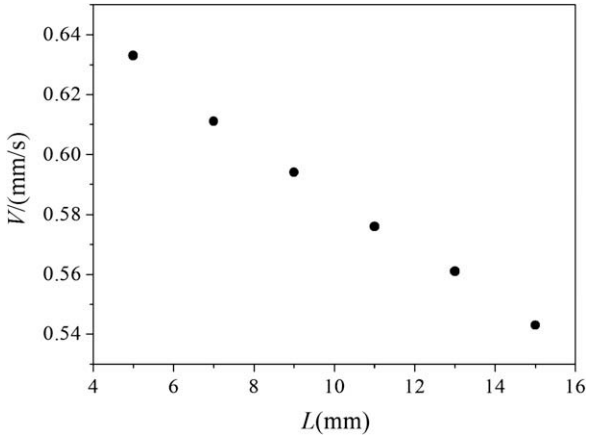

Fig. 10. Effect of the distance between the magnet and the loop on the flow velocity.

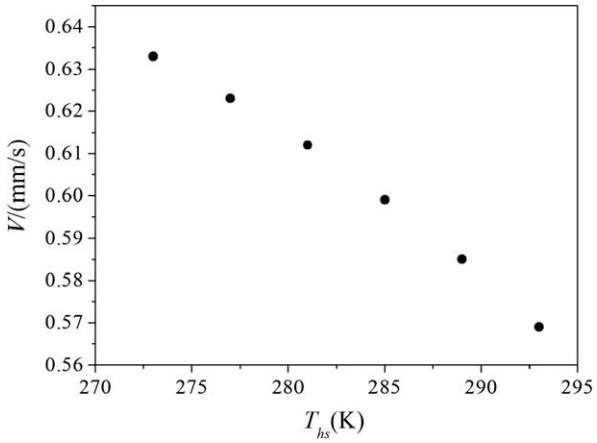

Fig. 8. Effect of heat sink temperature on the fluid flow velocity.

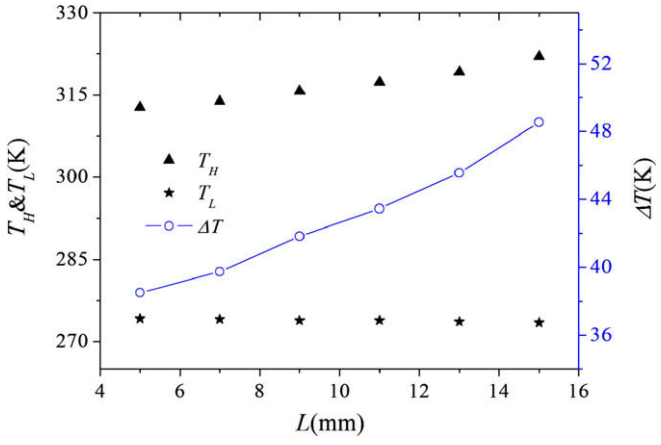

Fig. 11. Temperature variation with the distance between the magnet and the loop.

Table 2 gives the flow velocity values from the experimental and numerical approaches, respectively. Comparison shows satisfactory coincidence between the numerical values and experimental ones. Fig. 12 illustrates the measured and computational values of the fluid temperature at measuring points, in which position 1 and position 2 at the horizontal axis correspond to the inlet and outlet of the cooling section, position 3 and position 4 correspond to the inlet and outlet of the heating section, respectively. Evidently, a good match between the numerical and experimental values of the fluid temperature distribution is also reached.

Therefore, it can be stated that the experimental results validate the present theoretical model which can be used to predict perfor-

Table 2
Comparison between the experimental and numerical data for the flow velocity.

Operation conditions			Velocity comparison		
q (W/m^2)	T_{hs} (K)	L (mm)	V_{exp} (mm/s)	V_{num} (mm/s)	Error (%)
1000	273	5	0.338	0.379	11.8
2000	273	5	0.472	0.519	9.9
3000	273	5	0.612	0.633	3.4
4000	273	5	0.659	0.699	6.1
5000	273	5	0.802	0.751	6.4
3000	277	5	0.581	0.623	7.2
3000	281	5	0.537	0.611	12.1
3000	285	5	0.534	0.599	10.8
3000	273	7	0.577	0.611	5.5
3000	273	11	0.539	0.576	6.4
3000	273	13	0.511	0.561	8.9

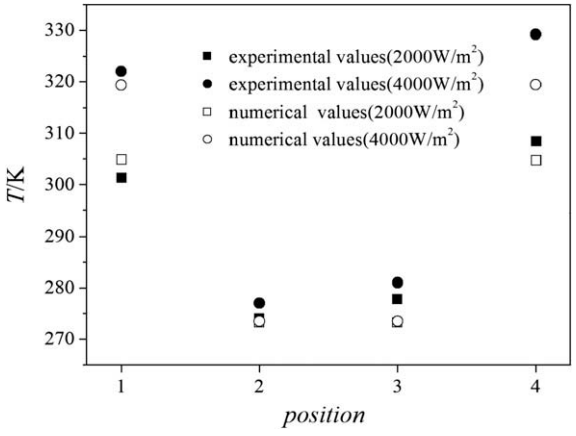

Fig. 12. Comparison between the experimental and numerical results for the fluid temperature.

mance of such automatic energy transport devices based on the thermomagnetic effect of temperature-sensitive magnetic fluid for design and evaluation purposes.

5. Conclusions

In this paper, a mathematical model has been established to predict flow and heat transport features of the temperature-sensitive magnetic fluid and to design an automatic energy transport device based on the thermomagnetic effect. A series of numerical simulations have been carried out to get insight into performance of such an energy conversion device. The results have revealed that a stable circulation flow can be maintained in a loop-shape channel in the presence of a proper external magnetic field and temperature gradient of the magnetic fluid. Among several factors influencing the device performance, the magnetic field strength and the fluid temperature difference between the heating section and cooling section are preponderant. It is not sufficiently high to warrant using such a device for heat-to-power energy conversion. However, since the flow can be easily controlled by the magnetic field and temperature distribution, and the device processes self-control function corresponding to the input heat load, it may be used as an automatically-cooling device as mentioned above.

The experimental results have been applied to estimate the present model. The model is validated by a good match between the numerical values and experimental results, revealing that this model can be used to simulate the performance of such devices exploiting the thermomagnetic effect for design and evaluation purpose.

Acknowledgment

This work is sponsored by the National Natural Science Foundation of China (Grant No. 50436020).

References

[1] S. Odenbach, Ferrofluids, Springer, Berlin, 2002.
[2] V.G. Bashtovoy, B.M. Berkovsky, A.N. Vislovish, Introduction to Thermomechanics of Magnetic Fluids, Hemisphere Publishing Corp., Washington, USA, 1988.
[3] A. Nethe, T. Schoppe, H. Stahlmann, Ferrofluid driven actuator for a left ventrical assist device, J. Magn. Magn. Mater. 201 (1999) 423–426.
[4] K. Raj, B. Moskowitz, R. Casciari, Advances in ferrofluid technology, J. Magn. Magn. Mater. 149 (1995) 174–180.
[5] B. Jeyadevan, C.N. Chinnasamy, K. Shinoda, K. Tohji, H. Oka, Mn–Zn ferrite with higher magnetization for temperature sensitive magnetic fluid, J. Appl. Phys. 93 (2003) 8450–8452.
[6] T. Upadhyay, R.V. Upadhyay, R.V. Mehta, V.K. Aswal, P.S. Goyal, Characterization of a temperature-sensitive magnetic fluid, Phys. Rev. B 55 (1997) 5585–5588.
[7] K. Nakatsuka, Y. Hama, J. Takahashi, Heat transfer in temperature-sensitive magnetic fluid, J. Magn. Magn. Mater. 85 (1990) 207–209.
[8] H. Matsuki, K. Yamasawa, K. Murakami, Experimental considerations on a new automatic cooling device using temperature-sensitive magnetic fluid, IEEE Trans. Magn. 13 (1977) 1143–1145.
[9] H. Yamaguchi, A. Sumiji, S. Shuchi, Characteristics of thermo-magnetic driven motor using magnetic fluid, J. Magn. Magn. Mater. 272–276 (2004) 2362–2364.
[10] K. Fumoto, H. Yamagishi, M. Ikegawa, A mini heat transport device based on thermo-sensitive magnetic fluid, Nanoscale Microscale Thermophys. Eng. 11 (2007) 201–210.
[11] J.L. Neuringger, R.E. Rosensweig, Ferrohydrodynamics, Phys. Fluids 7 (12) (1964) 1927–1937.
[12] Decai Li, Theory and Application of Magnetic Fluids, China Science Press, 2003. pp. 165–166 (in Chinese).
[13] R.E. Rosensweig, Ferrohydrodynamics, Cambridge University Press, Cambridge, UK, 1985.
[14] A.V. Farahani, A. Konrad, Demagnetizing factors for nonuniform nonlinear cylinders and rectangular prisms, IEEE Trans. Magn. 44 (11) (2008) 3225–3228.
[15] M. Beleggia, D. Vokoun, M.D. Graef, Demagnetization factors for cylindrical shells and related shapes, J. Magn. Magn. Mater. 321 (9) (2009) 1306–1315.
[16] M. Anhalt, B. Weidenfeller, L.J. Mattei, Inner demagnetization factor in polymer-bonded soft magnetic composites, J. Magn. Magn. Mater. (Netherlands) 320 (20) (2008) e844–e848.
[17] B.M. Berkovsky, Magnetic Fluids Engineering Applications, Oxford University Press, New York, USA, 1993.
[18] D.K. Wagh, A. Avashia, On the viscosity of a magnetic fluid, J. Magn. Magn. Mater. 153 (1996) 359–365.
[19] R. Patel, R.V. Upadhyay, R.V. Mehta, Viscosity measurements of a ferrofluid: comparison with various hydrodynamic equations, J. Colloid Interface Sci. 263 (2003) 661–664.
[20] C.Y. Chen, C.Y. Hong, S.W. Wang, Magnetic flows in a tube with the effects of viscosity variation, J. Magn. Magn. Mater. 252 (2002) 253–255.
[21] A.N. Vislovich, Phenomenological equation of static magnetization of magnetic fluids, Magnetohydrodynamics 26 (1990) 178–183.
[22] Q. Li, W.L. Lian, H. Sun, Y.M. Xuan, Investigation on operational characteristics of a miniature automatic cooling device, Int. J. Heat Mass Transfer 51 (2008) 5033–5039.
[23] W.L. Lian, Q. Li, Y.M. Xuan, Particle image velocimetry for an automatic cooling device using temperature-sensitive magnetic fluid, Sci. China E Technol. Sci. 51 (2008) 1203–1210.
[24] W.L. Lian, Q. Li, Y.M. Xuan, Characterization of miniature automatic energy transport devices based on the thermomagnetic effect, Energy Convers. Manage. 50 (2009) 35–42.